JACS
JOURNAL OF THE AMERICAN CHEMICAL SOCIETY
Article
pubs.acs.org/JACS

Coplanar Oligo(*p*-phenylenedisilenylene)s as Si=Si Analogues of Oligo(*p*-phenylenevinylene)s: Evidence for Extended π-Conjugation through the Carbon and Silicon π-Frameworks

Liangchun Li,[†] Tsukasa Matsuo,*[,†,∥,⊥] Daisuke Hashizume,[‡] Hiroyuki Fueno,[§] Kazuyoshi Tanaka,[§] and Kohei Tamao*[,†,#]

[†]Functional Elemento-Organic Chemistry Unit, RIKEN Advanced Science Institute, 2-1 Hirosawa, Wako, Saitama 351-0198, Japan
[‡]Materials Characterization Support Unit, RIKEN Center for Emergent Matter Science (CEMS), 2-1 Hirosawa, Wako, Saitama 351-0198, Japan
[§]Department of Molecular Engineering, Graduate School of Engineering, Kyoto University, Nishikyo-ku, Kyoto 615-8510, Japan
[∥]JST, PRESTO, 4-1-8 Honcho, Kawaguchi, Saitama 332-0012, Japan

Supporting Information

ABSTRACT: A series of oligo(*p*-phenylenedisilenylene)s (Si-OPVs **1**−**4**), silicon analogues of oligo(*p*-phenylenevinylene)s, up to the tetramer have been synthesized and isolated by the introduction of a newly developed protecting group [(HexO)MEind] for improving their solubility. The experimental and theoretical studies of the Si-OPVs **1**−**4** demonstrate the fully extended π-conjugation of the Si-OPV main chains. Single crystal X-ray analyses of the monomer **1** and the dimer **2** revealed the highly coplanar Si-OPV backbones facilitating the effective extension of the π-conjugation, which has further been validated by the significant increases in the absorption maxima from 465 nm for the monomer **1** to 610 nm for the tetramer **4**. The absorption maxima exhibit an excellent fit to Meier's equation, leading to the estimation of an effective conjugation length (ECL) of 9 repeat units (n_{ECL} = 9) and the absorption maximum of 635 nm for the infinite chain (λ_∞ = 635 nm). In sharp contrast to other nonemissive disilenes, the Si-OPVs **2**−**4** show an intense fluorescence from 613 to 668 nm at room temperature with the quantum yields up to 0.48. All the data presented here provide the first evidence for the efficient extended π-conjugation between the Si=Si double bonds and the carbon π-electron systems over the entire Si-OPV skeleton. This study reveals the possibility for developing the conjugated disilene π-systems, in which the Si=Si double bonds would be promising building blocks, significantly optimizing the intrinsic photophysical and electrochemical properties of the carbon-based π-conjugated materials.

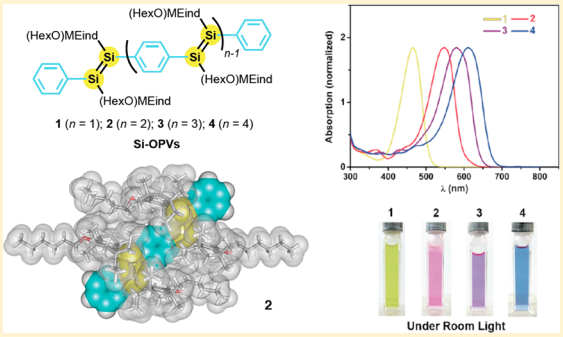

INTRODUCTION

The introduction of the heavier main group elements into organic π-conjugated systems has attracted considerable attention due to their potential applications in organic electronics.[1] Among them, the incorporation of multiple bonds of the heavier main group elements in the π-backbone would significantly optimize the electronic properties to possibly provide novel materials, but due to the limited synthetic approaches and their high reactivity, it is still a major challenge.[1a−c,f,g,2,3]

During the past few decades since 1981, when the concept of "kinetic stabilization" was introduced,[4] various stable unsaturated compounds possessing the heavier main group elements were prepared and isolated by using appropriately designed bulky protecting groups. In particular, compounds featuring multiple bonds of the heavier group 14 elements (Si, Ge, and Sn) have been extensively studied in order to obtain valuable insights into chemical bonding and their intrinsic properties in comparison to their sister analogues of carbon.[5]

Remarkable differences between disilenes ($R_2Si{=}SiR_2$) and alkenes ($R_2C{=}CR_2$) have been disclosed based on both experimental and computational studies.[5] Among them, two basic properties, from the energetic and structural points of view, should be discussed in terms of the "C=C—Si=Si conjugated system" attained by the introduction of the Si=Si double bond into the C=C π-conjugated system: (1) The Si=Si double bond involves the higher HOMO and the lower LUMO in comparison with the C=C double bond, resulting in the smaller HOMO−LUMO gap, about half that of the C=C double bond. This is basically due to the difference in the valence orbitals between carbon (2s and 2p) and silicon (3s and 3p). Whereas some unique properties would be anticipated in

Received: September 26, 2015
Published: November 11, 2015

DOI: 10.1021/jacs.5b10113
J. Am. Chem. Soc. 2015, 137, 15026−15035

the C═C—Si═Si systems, an important question is how efficiently the conjugation occurs between the C═C and Si═Si π-electron systems. (2) The Si═Si double bonds are conformationally flexible and thus feature planar, *trans*-bent, or twist geometries to some extent depending on the substituents. The currently reported disilenes exhibit bent angles θ (the angle between the Si═Si bond and R—Si—R plane) that range from 0 to 32.9° and the twist angles τ (the angle between two R—Si—R planes) that vary between 0 and 54.5° (Figure 1).[5]

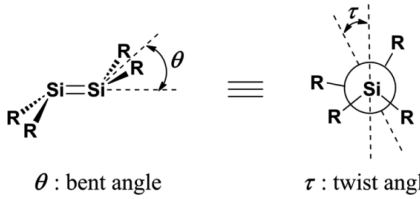

Figure 1. Schematic representation of the geometry of flexible disilenes.

This is ascribed to the balance between electronic and steric effects of the substituents, which have been theoretically elucidated by several models such as the Carter—Goddard—Malrieu—Trinquier[6] and Jahn—Teller distortion models.[5b,j,7]

If "coplanar C═C—Si═Si systems" are realized, we can obtain a deeper insight into the electronic structure, bonding nature, and the efficiency of the new π-conjugation frameworks. We have chosen the poly(*p*-phenylenedisilenylene)s (Si-PPV), Si═Si analogues of poly(*p*-phenylenevinylene)s (PPV), as the model for our study, primarily in light of the experimental viability.

Prior to the experimental work, we performed theoretical studies regarding the electronic structures of the PPV and Si-PPV models with hydrogen atoms on the vinylene and disilenylene moieties and with restriction of the planar disilene units and coplanar polymer skeletons, as shown in Figure 2 (B3LYP/6—21G(d,p)(5d functions) level; see the Supporting Information (SI) for details).

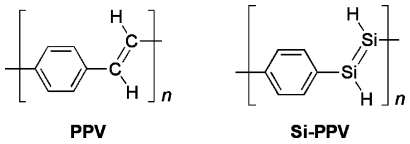

Figure 2. Structures of PPV and Si-PPV.

The representative results are summarized in Table 1, demonstrating the lower ionization potential (the higher top level of the highest occupied bands), the higher electron affinity (the lower bottom level of the lowest-unoccupied bands), and the smaller band gap for the Si-PPV, in comparison to those for the PPV. Thus, the theoretical results clearly predicted that the π-conjugation can be extended through the Si═Si double bonds and the phenyl(ene) groups in the ideal "coplanar" polymer framework.

Table 1. Electronic Properties of PPV and Si-PPV[a]

	PPV	Si-PPV
ionization potential[b]	4.672 (6.516)	4.512 (6.082)
electron affinity[b]	2.311 (−0.970)	2.526 (−0.297)
band gap[b]	2.361 (7.486)	1.986 (6.379)

[a]B3LYP/6-21G(d,p)(5d functions) level. In parentheses are shown the values by the Hartree—Fock framework for each polymer structure independently optimized under the same basis set 6-21G(d,p)(5d functions). [b]In eV.

How do we experimentally realize such a coplanar Si-PPV structure together with efficient protection of the reactive disilene moieties? The appropriately designed bulky protecting group is apparently the key for this objective. We have developed bulky fused-ring 1,1,3,3,5,5,7,7-octa-R-substituted *s*-hydrindacen-4-yl (abbreviated as Rind) groups,[2i,8] which have turned out to meet our present requirements (Figure 3).

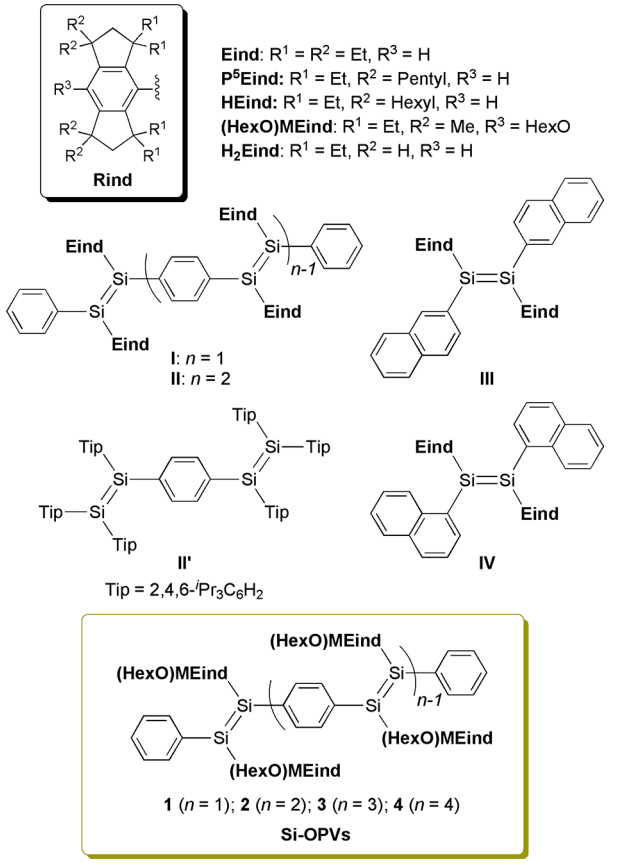

Figure 3. Structures of Rind groups and some representative disilene derivatives.

The Rind groups show a powerful potential to stabilize a variety of reactive species of boron, silicon, phosphorus, germanium, and so forth.[1a] Among them, the 1,2-diaryldisilene derivatives **I**—**IV** (Figure 3), protected by the Eind (R^1 = R^2 = Et, R^3 = H) groups, are found to be extremely air-stable. They also have highly coplanar π-frameworks surrounded by the perpendicularly oriented Eind groups.[2b—d,i] There was a remarkable change in the photophysical properties between the shorter members of the oligo(*p*-phenylenedisilenylene)s (Si-OPVs); yellow (absorption maximum λ_{max}^{abs} = 461 nm) and nonemissive **I** (n = 1) vs red (λ_{max}^{abs} = 543 nm) and room-temperature emissive (emission maximum λ_{max}^{em} = 612 nm) **II** (n = 2).[2i] In addition to **II**, which contains two disilene units on the central benzene ring, the 1,2-dinaphthyldisilenes **III** and **IV** containing two π-extended aromatic groups on one disilene unit exhibit an extensive red fluorescence even at room temperature.[2b,d] Based on these studies, we have demonstrated for the first time that the Si═Si chromophore can conjugate

DOI: 10.1021/jacs.5b10113
J. Am. Chem. Soc. 2015, 137, 15026—15035

with the carbon π-electron systems. We also tried to prepare the higher oligomers of Si-OPVs, but suffered from the limited solubility of the Eind-protected oligomers and no ^{1}H NMR spectrum of **II** was available.

We now report the successful isolation and full characterization of Si-OPVs **1**–**4** up to the tetramer by introducing an appropriately designed (HexO)MEind (R^1 = Et, R^2 = Me, R^3 = HexO) group with a hexyloxy chain at the *para* position of the MEind group (Figure 3), which significantly improves the solubility, enabling us to obtain further experimental evidence for the extended π-conjugation through the carbon and silicon π-frameworks including an effective conjugation length (ECL) and an absorption maximum for the infinite chain (λ_∞).

RESULTS AND DISCUSSION

Synthesis. We first attempted to synthesize the higher oligomers of Si-OPVs by introducing P^{5}Eind (R^1 = Et, R^2 = pentyl, R^3 = H) or HEind (R^1 = Et, R^2 = hexyl, R^3 = H) groups with four long alkyl chains at the peripheral benzylic positions (Figure 3).[8] While the solubility of the resulting oligomers seemed to be increased, their chromatographic separation became much harder because of their similar lower polarities. In addition, the formation of the higher oligomers seemed to be retarded probably due to the steric repulsion of the neighboring long alkyl chains.

We then designed the (HexO)MEind (R^1 = Et, R^2 = Me, R^3 = HexO) group by the incorporation of a long alkoxy chain at the *para* position of the MEind group, which will alleviate the repulsion between the bulky protecting groups and improve the solubility along with the increased polarity. This ligand design is based on one of the unique features of the Rind group, i.e., the availability of the *para* position for further functionalization.[1a,8]

Scheme 1. Synthesis of (HexO)MEind-Br

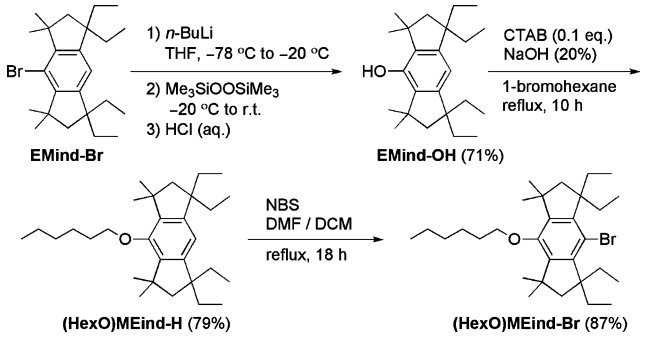

Scheme 2. Synthesis of Dibromosilane Derivatives 5 and 6

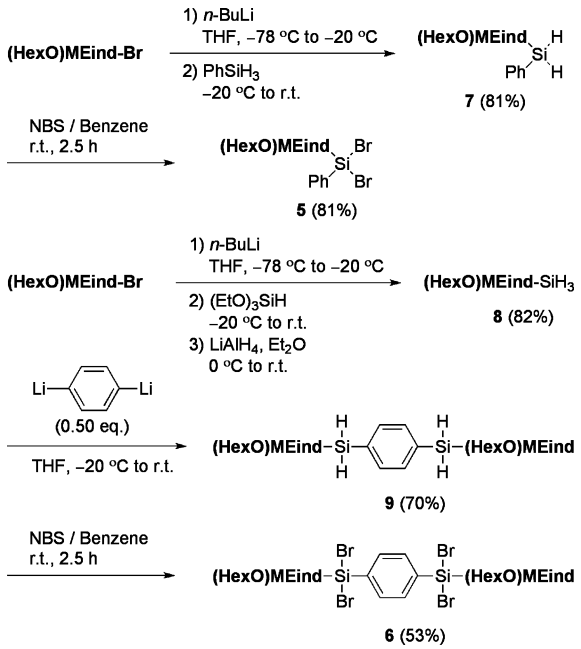

Scheme 3. Synthesis of Si-OPVs 1–4 by Reductive Coupling Reaction

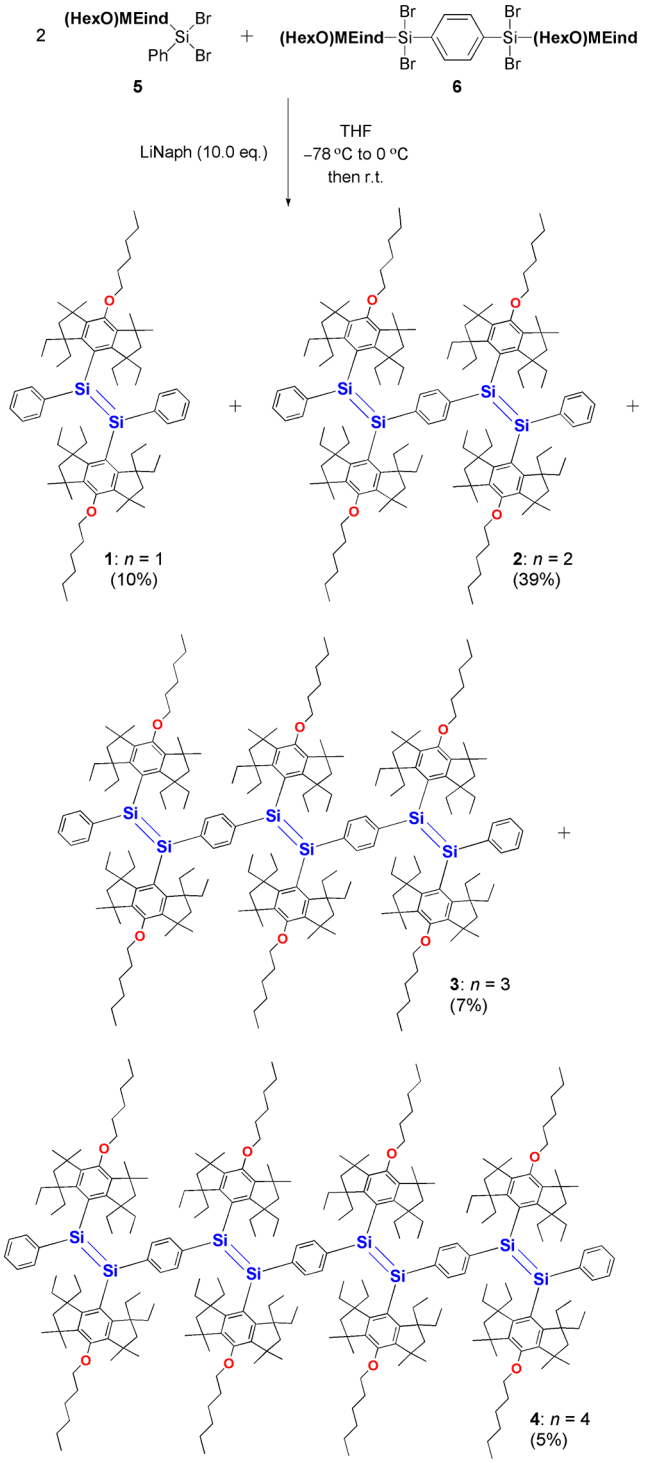

DOI: 10.1021/jacs.5b10113
J. Am. Chem. Soc. 2015, 137, 15026–15035

Table 2. NMR Spectroscopic Data, X-ray Structural Parameters, and HRMS Data for Si-OPVs 1−4, Together with Compounds II and II′

	1	2	3	4	II[a]	II′[b]
δ^{29}Si (ppm)	62.8	62.3, 63.4				56.8, 70.7
d(Si═Si) (Å)	2.1626(8)	2.1642(8)			2.156(2)	2.1674(8)
θ_{Si} (deg)[c]	1.65(8)	0.62(12), 3.38(13)			0.7(3), 2.7(3)	16.45(10), 19.31(10)
τ (deg)[c]	0.02(11)	2.79(17)			2.7(4)	3.44(14)
φ_{Ar} (deg)[d]		11.32(11)			9.0(3)	68.87(11)
M_{ex}[e]	1060.78926	2043.52857	3026.27527	4009.01611[f]		
M_{th}[g]	1060.78878	2043.53061	3026.27245	4009.01428		
Δ (ppm)[h]	0.45	−1.00	0.93	0.46		

[a]Data from ref 2i. [b]Data from ref 2j. [c]Bent angle θ_{Si} and twist angle τ have been defined in the Introduction. [d]Dihedral angle φ_{Ar} is defined as the angle between the central phenylene group and terminal aromatic rings. [e]Experimental value from the HRMS spectrometry. [f]Observed as $[M]^{2+}$. [g]Theoretical value. [h]$\Delta = [M_{ex} - M_{th}]10^6/M_{th}$.

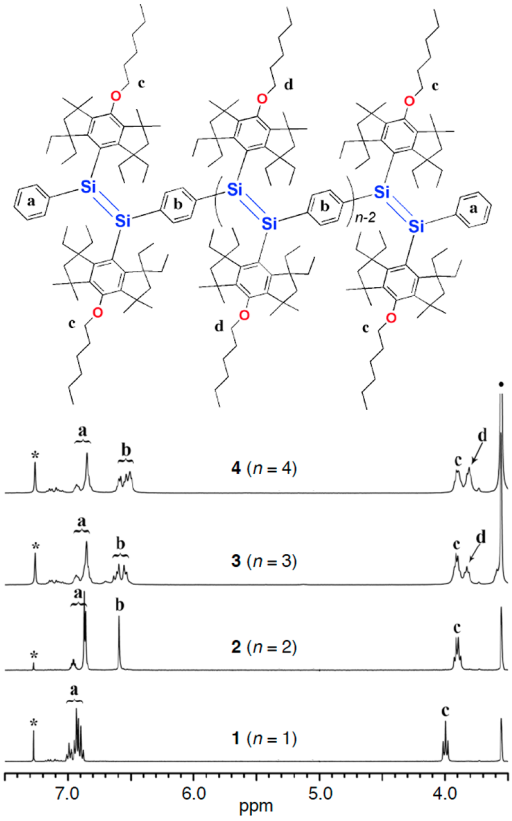

Figure 4. Assignment of the signals in the ^{1}H NMR spectra (3.5−7.5 ppm region) of Si-OPVs **1**−**4** in THF-d_8. Resonances: (●) residual solvent; (*) residual benzene; (a) terminal phenyl groups; (b) inner phenylene groups; (c) OCH_2 groups on the outer (HexO)MEind groups; and (d) OCH_2 group on the inner (HexO)MEind groups.

A bulky aryl bromide, (HexO)MEind-Br, can be prepared in four steps on a 10 g scale from the readily available EMind-Br as shown in Scheme 1 (see the SI for details). As expected, (HexO)MEind-Br shows a good solubility in common organic solvents, together with the higher polarity. For example, the R_f values on silica gel for the P^{5}Eind-Br, Eind-Br, and (HexO)-MEind-Br eluted with hexane are 0.82, 0.75, and 0.49, respectively.

Starting with (HexO)MEind-Br, two key substrates, the dibromosilane derivatives **5** and **6**, for the synthesis of the Si-OPVs were obtained by slightly modified routes as established for the synthesis of the Eind analogues,[2i] as shown in Scheme 2. The lithiation of (HexO)MEind-Br with *n*-BuLi followed by the addition of phenylsilane ($PhSiH_3$) gave the dihydrosilane **7** in 81% yield, which was used for the subsequent bromination with *N*-bromosuccinimide (NBS) in benzene to afford an almost pure dibromosilane **5** in 81% crude yield. For the synthesis of 1,4-bis(dibromosilyl)benzene **6**, trihydrosilane **8** was obtained in 82% yield by the treatment of (HexO)MEind-Li with triethyoxylsilane $(EtO)_3SiH$ followed by the reduction with $LiAlH_4$ in Et_2O. The reaction of **8** with 1,4-dilithiobenzene, freshly prepared from 1,4-dibromobenzene and *t*-BuLi, afforded 1,4-bis(dihydrosilyl)benzene **9** as colorless crystals in 70% yield after recrystallization from EtOH. Finally, compound **9** was brominated with NBS in benzene to afford **6** in 53% yield.

With **5** and **6** in hand, we then carried out a one-pot reductive coupling reaction with lithium naphthalenide (LiNaph) to prepare the Si-OPVs, as shown in Scheme 3. For the construction of the Si-OPVs framework, dibromosilane **5** and 1,4-bis(dibromosilyl)benzene **6** will be an end-capping unit and a central building unit, respectively. Thus, the molar ratio of the reactants of **5** and **6** and a dose of lithium naphthalenide (LiNaph) were crucial for the formation of the desired products to minimize any side products. We screened various reaction conditions and finally found the optimal conditions. A slow addition of a toluene solution of a mixture of **5** and **6** in a 2:1 ratio to a freshly prepared LiNaph (ca. 10 equiv) in THF at −78 °C yielded a purple mixture from which the Si-OPVs **1**−**4** up to a tetramer were able to be separated. Albeit we finally succeeded in isolating the four oligomers **1**−**4**, their complete separation from the reaction mixture was a hard and challenging task. Since the resulting Si-OPVs in solution are sensitive to air and moisture, all the manipulations were carried out under an argon atmosphere or in an argon-filled glovebox, and all the glassware, silica gel, and solvents were required to ensure the exclusion of air and moisture. In addition, a large amount of eluents were necessary during the silica gel column chromatography due to the still poor solubility of the trimer **3** and the tetramer **4** even in THF (see the SI for details). Under the fine-tuned reaction conditions and the careful separation processes, a total isolated yield of the Si-OPVs **1**−**4** was reached 61% based on **5**.

Characterization. The monomer **1** and the dimer **2** were fully characterized by multinuclear NMR spectroscopy (^{1}H, ^{13}C, and ^{29}Si), high resolution mass spectrometry (HRMS), and X-ray crystallography, while the trimer **3** and the tertramer **4** were probed by ^{1}H NMR spectroscopy and HRMS. Table 2 summarizes the ^{29}Si NMR data, structural parameters determined by X-ray crystallography, and HRMS data for **1**−

DOI: 10.1021/jacs.5b10113
J. Am. Chem. Soc. 2015, 137, 15026−15035

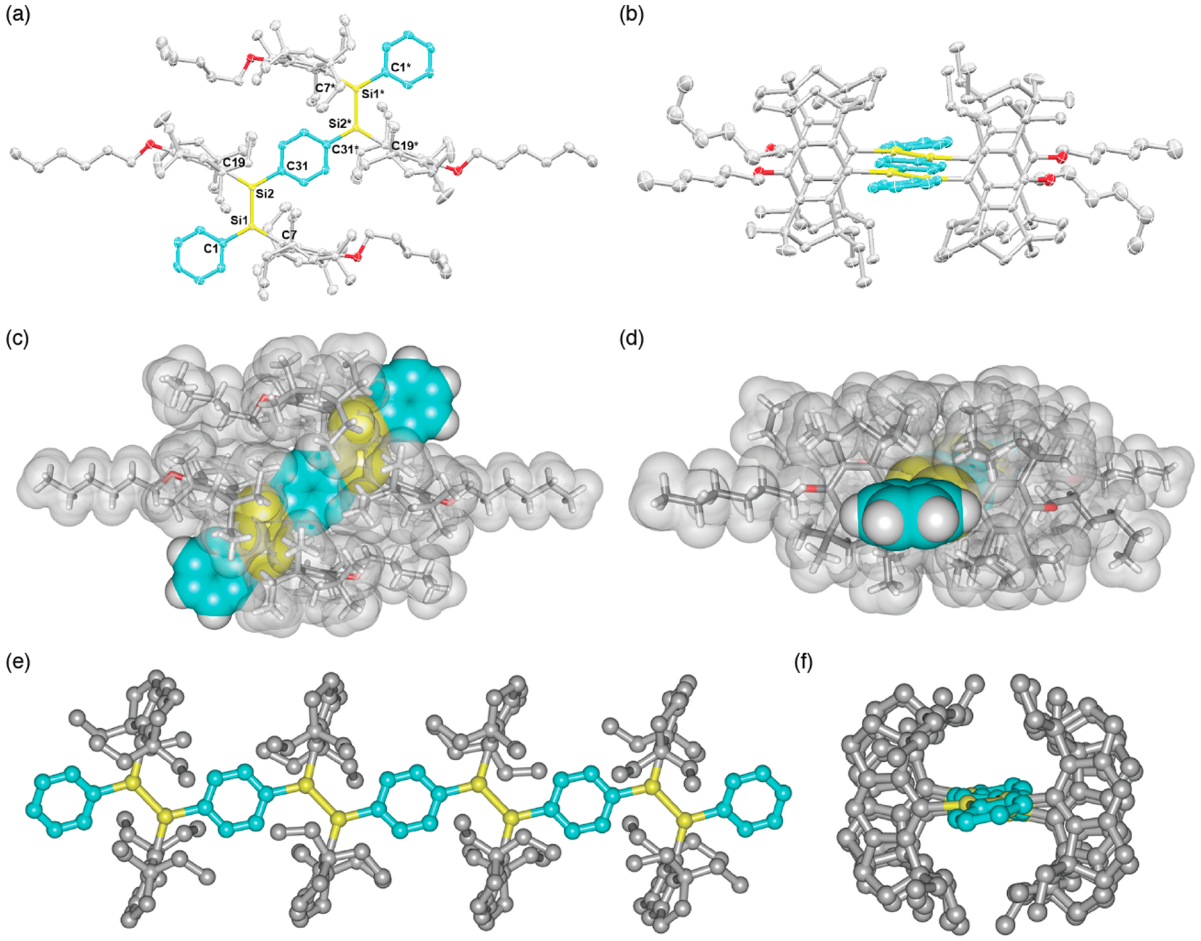

Figure 5. Crystal structures of **2** (50% probability for thermal ellipsoids): (a) top view and (b) front view; hydrogen atoms and disordered groups are omitted for clarity. Selected bond lengths (Å) and bond angles (deg): Si1−Si2 = 2.1642(8), C1−Si1 = 1.868(2), C7−Si1 = 1.893(2), C19−Si2 = 1.894(2), C31−Si2 = 1.864(2), C1−Si1−C7 = 121.43(10), C1−Si1−Si2 = 118.62(8), C7−Si1−Si2 = 119.84(7), C19−Si2−Si1 = 121.36(7), C19−Si2−C31 = 119.29(10), C31−Si2−Si1 = 119.34(8); (c) top view and (d) front view with the van der Waals surface in light gray color. The phenyl and phenylene groups are shown with light-blue space-filling model: silicon, yellow; oxygen, red; carbon, gray; hydrogen, white. Theoretically optimized structure of tetramer **4′** with simplified H_2Eind protecting groups: (e) top view and (f) front view in ball-and-stick model; hydrogen atoms are omitted for clarity.

4, together with some pertinent data for **II** and Scheschkewitz's compound **II′** for comparison.

HRMS Data. As listed in Table 2, the most reliable evidence for the formation of the Si-OPVs comes from the HRMS data (M_{ex}) that qualitatively matched with the theoretical values (M_{th}) within the measurement error (Δ) of 1 ppm. Strong parent ions $[M]^+$ for **1**−**3** and a strong doubly charged ion $[M]^{2+}$ for **4** are observed in the electrospray mass spectra (see the SI).

^{1}H NMR Data. The lower field region (3.5−7.5 ppm) of the ^{1}H NMR spectra of **1**−**4** is reproduced in Figure 4. All the ^{1}H signals could be well assigned; the integrals of all the resonances are fully consistent with the number of corresponding protons. Compared with the peaks (a) at the lowest magnetic field region around 7.0 ppm assignable to the terminal phenyl group, the signals (b) (around 6.6 ppm) of the inner phenylene group are slightly upfield shifted due to the shielding effects by the surrounding (HexO)MEind groups (vide infra). The resonances (c and d) assignable to the OCH_2 protons can act as an internal standard. Thus, while only one well-resolved peak (c) appears in the spectra of **1** and **2**, a couple of signals (c and d) are observed around at 3.8 and 3.9 ppm in the spectra of **3** and **4**, thus being in accordance with the existence of the inner and outer (HexO)MEind groups. The proton integral ratio of the signals (a−d) is 5:4:4:2 for **3** and 5:6:4:4 for **4**, which are in good agreement with the target molecular structures.

^{29}Si NMR Data. As shown in Table 2, in the ^{29}Si NMR spectra, two signals at 62.3 and 63.4 ppm are observed for the dimer **2**, which are close to that for **1** (62.8 ppm), in the range of those for typical aryl-substituted disilenes.[9] The close ^{29}Si shifts suggest a similar Si environment in a highly coplanar Si-OPV framework. We also tried to observe the ^{29}Si signals for **3** and **4**, however, no detectable peak was found despite a prolonged measurement, probably due to the lower solubility of **3** and **4** relative to **1** and **2**.

X-ray Crystallography. The molecular structures of **1** (Figure S3) and **2** (Figure 5) exhibit an entirely coplanar geometry with a very small bent angle (θ_{Si}) of ca. 0.6−3.4° and a twist angle (τ) of ca. 0.0−2.8° and with a dihedral angle (φ_{Ar}) in **2** between the central and terminal benzene rings of ca. 11° (Table 2). As shown in Figure 5, similar to the Eind protected Si-OPV dimer **II**, the highly coplanar Si═Si−phenyl(ene) core framework is fixed by the perpendicularly oriented (HexO)-MEind groups, as visualized by the front view. In other words, each of the rigid (HexO)MEind ligands possessing four ethyl

DOI: 10.1021/jacs.5b10113
J. Am. Chem. Soc. 2015, 137, 15026−15035

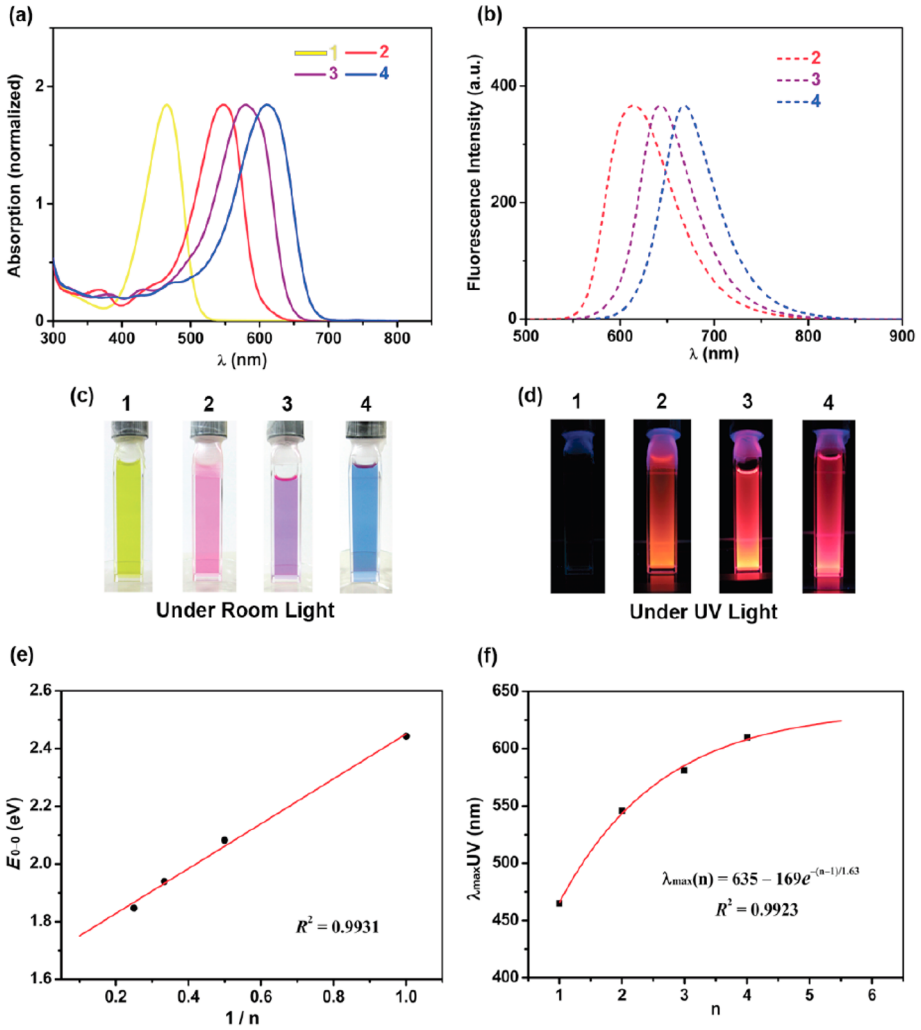

Figure 6. (a) UV−vis absorption and (b) fluorescence spectra of Si-OPVs **1**−**4** in THF at room temperature. Photographs of the THF solutions of **1**−**4**: (c) under room light and (d) under 360 nm UV light. (e) Linear plot of the 0−0 transition energies against $1/n$. (f) Exponential fit of absorption data.

Table 3. Photophysical Data for Si-OPVs 1−4

	λ_{max}^{abs} (nm) [ε (cm^{-1} M^{-1})][ab]	λ_{max}^{em} (nm)[ac]	$\Delta\nu_{Stokes}$ (cm^{-1})[d]	Φ_F[e]	τ (ns)[f]	τ_n^{calcd} (ns)[g]	τ_n^{exp} (ns)[h]	k_r (s^{-1})[i]	k_{nr} (s^{-1})[i]	E_{0-0} (eV)[j]
1	465 [2.8×10^4]	n.d.		n.d.						2.44
2	546 [4.3×10^4]	613	2000	0.11	1.8[k]	8.6	16.4	6.1×10^7	4.9×10^8	2.08
3	581 [5.0×10^4]	643	1660	0.46	2.5	8.0	5.4	1.8×10^8	2.2×10^8	1.94
4	610 [7.1×10^4]	668	1420	0.48	2.2	6.9	4.6	2.2×10^8	2.4×10^8	1.85

[a]Measured in oxygen- and moisture-free THF at room temperature. [b]Absorption maximum (λ_{max}^{abs}). [c]Emission maximum (λ_{max}^{em}), excited at (λ_{max}^{abs}) −40 nm. [d]Stokes shift ($\Delta\nu_{Stokes}$). [e]Absolute fluorescence quantum yield (Φ_F). [f]Fluorescence lifetime (τ) measured by the time-correlated single-photon counting (TCSPC) operation mode at photoexcitation wavelength of 590 nm. [g]Calculated natural lifetimes (τ_n^{calcd}) derived from the inherent radiative rate constant k_e^0, $\tau_n^{calcd} = 1/k_e^0$; see the SI for details, ref 11. [h]Natural lifetimes (τ_n^{exp}) estimated by $\tau_n^{exp} = \tau/\Phi_F$. [i]Radiative rate constant (k_r) calculated as $k_r = \Phi_F/\tau$, and nonradiative rate constant (k_{nr}) calculated as $k_{nr} = (1 - \Phi_F)/\tau$. [j]The 0−0 transition energy (E_{0-0}) calculated from the onset wavelength of the absorption spectrum. [k]The fluorescent decay of **2** exhibits a better fit to the biexponential function in which τ_1 and τ_2 were estimated to be 1.0 and 2.3 ns with 40% and 60% contributions, respectively, and thus, an average lifetime (ref 11) is given.

groups arranges side by side to create a cuboid tunnel, which is tailored to perfectly hold the flexible disilene moieties connected with a phenylene bridge. While the two disilene moieties are completely encapsulated, the benzene rings including the central phenylene group are partly covered by the ligands in view of the van der Waals surface models (Figure 5c and d). Whereas single crystals of the trimer **3** and tetramer **4** suitable for X-ray analysis were not obtained due to their poor crystallinity, the theoretically optimized structure (vide infra) of a model system of tetramer **4′** with simplified H_2Eind groups (Figure 3) is shown in Figure 5e and f for comparison, strongly suggesting the coplanar core framework also in this elongated oligomer.

Photophysical Properties. The most important feature of these Si-OPVs is their high coplanarity, which whether retained or not with the increasing chain length is obviously important to be experimentally clarified. We have now estimated the effective conjugation length (ECL) based on the photophysical

DOI: 10.1021/jacs.5b10113
J. Am. Chem. Soc. 2015, 137, 15026−15035

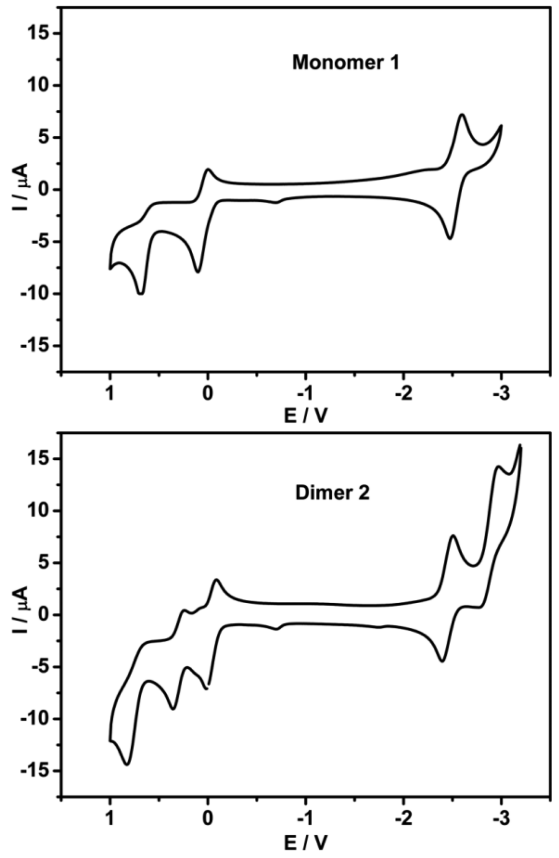

Figure 7. Cyclic voltammograms of **1** (top) and **2** (bottom) recorded in a THF solution using $[Bu_4N][PF_6]$ as the supporting electrolyte, a glassy carbon disk as the working electrode, a Pt wire as the counter electrode, and a Ag/Ag^+ ($AgNO_3$ in MeCN) as the reference electrode. Scan rate = 100 mV/s.

Table 4. Electrochemical Data for 1 and 2, Together with Compounds II′,[a] $(Mes)_2Si{=}Si(Mes)_2$,[c] and $(Tip)_2Si{=}Si(Tip)_2$[c]

compd	E_{ox} (V) vs Fc/Fc^+	E_{red} (V) vs Fc/Fc^+
1	−0.20, 0.42 (irre.)	−2.79
2	−0.30, 0.03, 0.58 (irre.)	−2.72, −3.24 (irre.)
II′[b]	−0.35 (irre.)	−2.70, −3.02
$(Mes)_2Si{=}Si(Mes)_2$[c]	+0.44 (+0.38)[d]	
$(Tip)_2Si{=}Si(Tip)_2$[c]	+0.56, +1.32	−2.66

[a]The potentials are relative to the ferrocene/ferrocenium (Fc/Fc^+). [b]Data from ref 2j. [c]Data from ref 15: Mes = 2,4,6-trimethylphenyl, Tip = 2,4,6-tri(isopropyl)phenyl. [d]Data from ref 14.

properties. The spectral properties of the Si-OPVs **1**−**4** are shown in Figure 6, and their photophysical data are summarized in Table 3.

Absorption. As shown in Figure 6a, the absorption maxima (λ_{max}^{abs}) of **1**−**4** exhibited at 465, 546, 581, and 610 nm, respectively, associated with the extremely high molar extinction coefficients ($\varepsilon = 2.8-7.1 \times 10^4$ cm^{-1} M^{-1}) assignable to the $\pi-\pi^*$ transition. The color changes from yellow to blue as shown in Figure 6c. The significant bathochromic shifts concurring with the increasing repeat units could be rationalized to the extended π-conjugation of the Si-OPVs. Thus, it is plausible that the coplanarity of **3** and **4** is retained to facilitate the efficient π-conjugation of the entire Si-OPVs backbone.

Emission. As shown in Figure 6b and d, except for the monomer **1**, the dimer to tetramer **2**−**4** show a bright orange or red fluorescence with emission maximum (λ_{max}^{em}) from 613 to 668 nm at room temperature. The quantum yields (Φ_F) of **2**−**4** progressively increase from 0.11 to 0.48 (Table 3). The Stokes shifts ($\Delta\nu_{Stokes}$) for **2**−**4** gradually decrease from 2000 to 1420 cm^{-1} which are lower than that of the flexible carbon-based OPVs (3199−3029 cm^{-1})[10a] and higher than that of the very rigid carbon-bridged OPVs (772−583 cm^{-1}),[10b] indicative of the relative structural rigidity of the Si-OPVs, primarily ascribed to the rather rigid cuboid tunnel created by the perpendicularly fixed (HexO)MEind groups.

Fluorescence Lifetimes. As shown in Table 3, the fluorescence lifetimes (τ) are 1.8−2.5 ns for **2**−**4** irrespective of the chain length, whereas the natural lifetimes (τ_n^{exp}, estimated from τ and Φ_F) become shorter with the increasing chain length.[11] The calculated natural lifetimes (τ_n^{calcd}) show the same trend and are comparable to the τ_n^{exp} values.[12] In addition, the radiative rate constants (k_r) of **2**−**4** increase from 6.1×10^7 to 2.2×10^8 s^{-1} contributing to the increasing quantum yields, while the nonradiative rate constants (k_{nr}) reduce to approximately a half from the dimer **2** to the higher oligomers **3** and **4** (see the SI for details).

Effective Conjugation Length (ECL). As shown in Figure 6e, the 0−0 transition energies (E_{0-0}) estimated from the absorption spectra are plotted versus $1/n$, where n is the number of repeat units. The fitting gives an excellent linear correlation (R^2 = 0.993) with an intercept of 1.67 eV corresponding to the energy of the Si-OPV polymer with an infinite chain, that is, $n \rightarrow \infty$ (imaginary Si-PPV). However, as Meier pointed out, this extrapolation is not suitable for higher oligomers reaching the ECL.[13] To gain further insight into the π-conjugation feature of our Si-OPV systems, our experimental absorption maxima data (black squares in Figure 6f) are fitted to Meier's equation to get the red curve line in Figure 6f. The good fitting with the experimental data (R^2 = 0.992) leads to the estimation of the absorption maximum of the infinite chain, λ_∞ = 635 nm (1.95 eV), and the effective conjugation length (ECL), n_{ECL} = 9 repeat units (see the SI for details).

In summary, the aforementioned photophysical properties of the Si-OPVs are remarkably different from their parent carbon system OPVs, oligo(*p*-phenylenevinylene)s.[10a,13] The following several points are worthy of note: (i) Both the absorption and emission maxima (λ_{max}^{abs} = 465−610 and λ_{max}^{em} = 613−668 nm) of the Si-OPVs are much longer than those of the carbon-based OPVs monomer to tetramer λ_{max}^{abs} = 354−450 and λ_{max}^{em} = 413−521 nm).[13] (ii) The Stokes shifts of the Si-OPVs ($\Delta\nu_{Stokes}$ = 2000−1420 cm^{-1}) are about 1200 cm^{-1} lower than those of the OPVs ($\Delta\nu_{Stokes}$ for the OPVs dimer to tetramer are 3199−3029 cm^{-1}).[13] (iii) The derived λ_∞ value of 635 nm for the Si-OPVs is 154 nm longer than that for the OPVs (λ_∞ = 481 nm), and the effective conjugation length (n_{ECL} = 9) for the Si-OPVs is shorter than that for the OPVs (n_{ECL} = 11). Thus, the incorporation of the Si═Si units into the carbon π-conjugated systems will significantly change the absorption and emission over a wide range and efficiently optimize the photophysical properties of the parent systems.

Electrochemical Properties. The electrochemical features of **1** and **2** were investigated by cyclic voltammetry (CV) in an oxygen-free and anhydrous THF at room temperature in an argon-filled glovebox. The Si-OPV solutions contained $[Bu_4N]$-

DOI: 10.1021/jacs.5b10113
J. Am. Chem. Soc. 2015, 137, 15026−15035

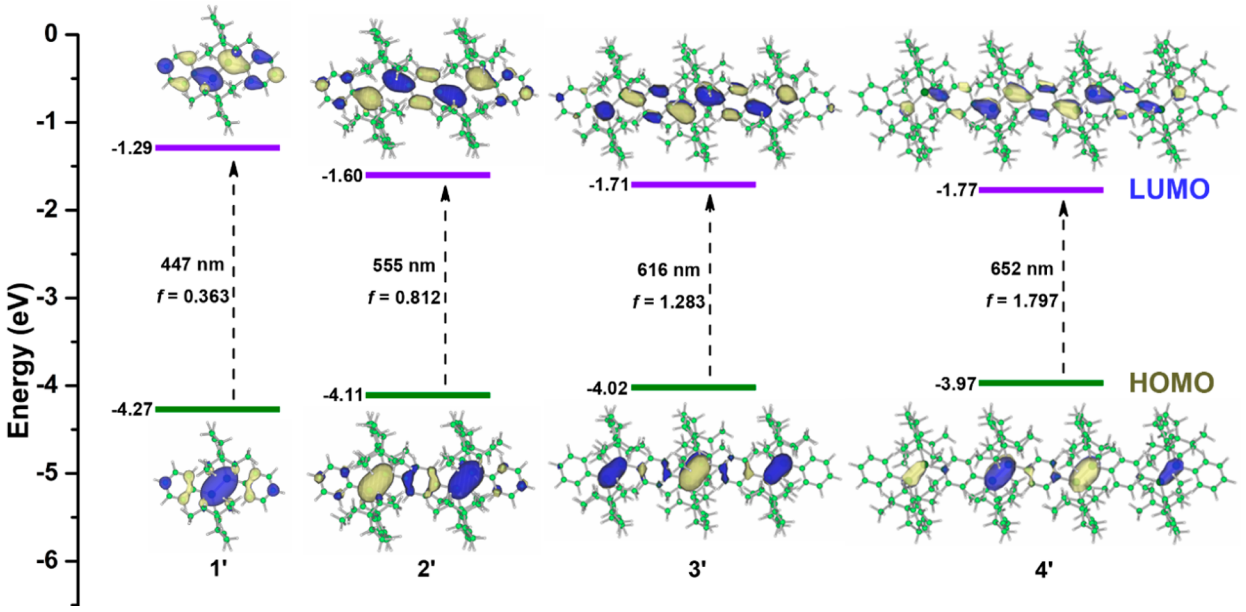

Figure 8. Frontier molecular orbital diagrams of model compounds **1′**−**4′** and the major electronic transitions.

$[PF_6]$ as the supporting electrolyte, and ferrocene was used as an external reference. No change was observed in the CV curves within subsequent scan cycles, indicating a good electrochemical stability. Unfortunately, the cyclic voltammograms of **3** and **4** were not available due to their low solubility in THF. The CV curves of compounds **1** and **2** are shown in Figure 7, and the electrochemical data are summarized in Table 4 together with those of **II′**,[2j] $Mes_2Si{=}SiMes_2$ (Mes = 2,4,6-trimethylphenyl),[14,15] and $Tip_2Si{=}SiTip_2$ (Tip = 2,4,6-triisopropylphenyl)[15] for comparison.

The monomer **1** and dimer **2** show a reversible first reduction wave, tentatively assignable to the disilene unit reduction. The first reduction potential for **2** (−2.72 V) is similar to that for **II′** (−2.70 V) and somewhat higher than that of **1** (−2.79 V), indicative of a lower LUMO energy level for **2** relative to that for **1**. This reduction coincides with the results that **1** shows only one while the dimers **2** and **II′** display two reduction potentials. The first oxidation potentials located at −0.30 V for **2** and −0.35 V for **II′** are comparable but lower than that for **1** (−0.20 V), suggesting a higher HOMO level of the dimers due to the extended π-conjugation including the central *p*-phenylene group. The two tetraaryldisilenes, $Mes_2Si{=}SiMes_2$ and $Tip_2Si{=}SiTip_2$, have much higher oxidation potentials shifting anodically about +0.6−0.7 V in comparison with **1**, indicating a significantly lower HOMO level, probably due to less efficient π-conjugation in the twisted disilenes with four bulky aryl groups.

Theoretical Studies. In order to shed light on the electronic nature of these disilenes, and in particular, to obtain a better understanding of the extended π-conjugation features, density functional theory (DFT) calculations were performed at the B3LYP/6-31G(d,p) level for the simplified model Si-OPVs **1′**−**4′**, in which the (HexO)MEind groups are replaced by H_2Eind groups (Figure 3). The HOMO and LUMO orbital diagrams and energy levels are shown in Figure 8. The geometry optimizations were carried out using the Gaussian 09 program package[16] with constraint of C_i symmetry. The Wiberg bond index (WBI)[17] and natural population analysis (NPA)[18] charge distribution were calculated by the natural bond orbital method. Time-dependent DFT (TD-DFT) calculations were subsequently performed for the absorptions at the ground-state geometry using the TD-B3LYP/6-31G(d,p) method. The contributions of the transitions were estimated by the oscillator strengths (*f*) and the first 24 singlet and triplet states were calculated. The selected parameters are presented in Figure 8 (for more details, see the SI).

The optimized structures of **1′** and **2′** well reproduce the corresponding X-ray structures. The calculated Si=Si bond distances of **1′**−**4′** are in the range of 2.1771−2.1871 Å which are reasonably close to the experimental values. The WBI of the Si−Si bonds are 1.660−1.689, indicating the double bond character. The NPA charge distributions show positive Si atoms (ca. +0.8) and negative Si-bonded C atoms (ca. −0.5) (see the SI). As shown in Figure 8, the HOMOs are prominently located on the Si=Si bonds, while the LUMOs delocalize over the entire Si-OPV chains. From the monomer **1′** to tetramer **4′**, the contributions from the phenyl and phenylene groups to the HOMOs are considerably decreased to be almost negligible in the tetramer **4′** and the significant participations from the terminal phenyl groups to the LUMOs progressively decrease. With the repeat units increasing, the HOMO levels increase from −4.27 to −3.97 eV, and the LUMO levels simultaneously decrease from −1.29 to −1.77 eV. The resulting overall decrease in the energy gap from ca. 2.98 to 2.20 eV is in good agreement with the trends observed in the UV−vis spectra (Table 3), which further supports the fact that the π-conjugation extends over the entire Si-OPV skeletons. It is also notable that the energy gap for the tetramer **4′** (2.20 eV) is smaller than the band gap for the carbon-based ideal polymer PPV (2.361 eV) and approaches the band gap of the silicon analogue Si-PPV (1.986 eV), as discussed in the introductory remarks (see Table 1).

The TD-DFT calculations reproduce the experimental absorption spectra of **1′**−**4′** with a similar single-band centered at 447, 555, 616, and 652 nm, respectively (also see the SI). These absorption maxima mainly assignable to the HOMO → LUMO ($\pi \rightarrow \pi^*$) transitions are reasonably in accordance with the already mentioned experimental results. These calculations

DOI: 10.1021/jacs.5b10113
J. Am. Chem. Soc. 2015, 137, 15026−15035

thus support the experimental results and consolidate the interpretations of the photophysical and electrochemical properties of the Si-OPVs.

CONCLUSIONS

By developing a new bulky ligand, (HexO)MEind, possessing an improved solubility and higher polarity, a series of Si-OPVs have been synthesized and separated by careful column chromatography to obtain the monomer to tetramer **1**−**4** in the pure state. The highly coplanar Si═Si−phenyl(ene) core frameworks protected by the perpendicularly fixed (HexO)-MEind groups have been demonstrated in the monomer **1** and the dimer **2** by X-ray crystallography. The photophysical and electrochemical properties and theoretical calculations provide strong evidence for the extended π-conjugation through the coplanar Si═Si−phenyl(ene) backbone over the entire Si-OPV chain. The effective conjugation length (ECL) has been estimated based on Meier's equation to be nine repeat units.

As mentioned in the Introduction, we have recently reported a trial for the application of the air-stable, room temperature emissive di(2-naphthyl)disilene **III** as an emissive material in OLEDs, which has opened a small door to a new field for application of the "C═C—Si═Si conjugated system".[2c] We hope that the present study would also provide a new challenge for application of the "C═C—Si═Si conjugated polymer".

ASSOCIATED CONTENT

Supporting Information

The Supporting Information is available free of charge on the ACS Publications website at DOI: 10.1021/jacs.5b10113.

Experimental details, details of the measurements, and calculations (PDF)
Crystallographic data for (HexO)MEind-Br (CIF)
Crystallographic data for compound **1** (CIF)
Crystallographic data for compound **2** (CIF)

AUTHOR INFORMATION

Corresponding Authors

*t-matsuo@apch.kindai.ac.jp
*tamao@riken.jp

Present Addresses

[⊥]Department of Applied Chemistry, Faculty of Science and Engineering, Kinki University, 3-4-1 Kowakae, Higashi-Osaka, Osaka 577-8502, Japan.
[#]RIKEN Global Research Cluster, 2-1 Hirosawa, Wako, Saitama 351-0198, Japan.

Notes

The authors declare no competing financial interest.

ACKNOWLEDGMENTS

This study was supported by the Ministry of Education, Culture, Sports, Science, and Technology of Japan for the Grant-in-Aid for Specially Promoted Research (No. 19002008). The numerical calculations were partly performed at the Research Center for Computational Science, Okazaki, Japan. We thank Dr. A. Fukazawa (Nagoya University) for her valuable discussion and Dr. Y. Hongo and Dr. T. Nakamura (RIKEN CSRS) for their kind help with the mass spectrometry. We are grateful to the materials characterization support unit, RIKEN CEMS for the elemental analyses.

REFERENCES

(1) Some pertinent reviews: (a) Matsuo, T.; Tamao, K. *Bull. Chem. Soc. Jpn.* **2015**, *88*, 1201−1220. (b) Simpson, M. C.; Protasiewicz, J. D. *Pure Appl. Chem.* **2013**, *85*, 801−815. (c) Matsuo, T.; Kobayashi, M.; Tamao, K. *Dalton Trans.* **2010**, *39*, 9203−9208. (d) Matsuo, T.; Li, B.; Tamao, K. *C. R. Chim.* **2010**, *13*, 1104−1110. (e) Fukazawa, A.; Yamaguchi, S. *Chem. - Asian J.* **2009**, *4*, 1386−1400. (f) Grimsdale, A. C.; Müllen, K. *Macromol. Rapid Commun.* **2007**, *28*, 1676−1702. (g) Baumgartner, T.; Reau, R. *Chem. Rev.* **2006**, *106*, 4681−4727. (h) Gates, D. P. *Top. Curr. Chem.* **2005**, *250*, 107−126. (i) Hissler, M.; Dyer, P. W.; Reau, R. *Top. Curr. Chem.* **2005**, *250*, 127−163. (j) Yamaguchi, S.; Tamao, K. *Chem. Lett.* **2005**, *34*, 2−7. (k) Hissler, M.; Dyer, P. W.; Reau, R. *Coord. Chem. Rev.* **2003**, *244*, 1−44. (l) Yamaguchi, S.; Tamao, K. *J. Chem. Soc., Dalton Trans.* **1998**, 3693−3702.

(2) Si═Si (a) Sakagami, M.; Sasamori, T.; Sakai, H.; Furukawa, Y.; Tokitoh, N. *Bull. Chem. Soc. Jpn.* **2013**, *86*, 1132−1143. (b) Kobayashi, M.; Hayakawa, N.; Nakabayashi, K.; Matsuo, T.; Hashizume, D.; Fueno, H.; Tanaka, K.; Tamao, K. *Chem. Lett.* **2014**, *43*, 432−434. (c) Tamao, K.; Kobayashi, M.; Matsuo, T.; Furukawa, S.; Tsuji, H. *Chem. Commun.* **2012**, *48*, 1030−1032. (d) Kobayashi, M.; Matsuo, T.; Fukunaga, T.; Hashizume, D.; Fueno, H.; Tanaka, K.; Tamao, K. *J. Am. Chem. Soc.* **2010**, *132*, 15162−15163. (e) Jeck, J.; Bejan, I.; White, A. J. P.; Nied, D.; Breher, F.; Scheschkewitz, D. *J. Am. Chem. Soc.* **2010**, *132*, 17306−17315. (f) Sato, T.; Mizuhata, Y.; Tokitoh, N. *Chem. Commun.* **2010**, *46*, 4402−4404. (g) Yuasa, A.; Sasamori, T.; Hosoi, Y.; Furukawa, Y.; Tokitoh, N. *Bull. Chem. Soc. Jpn.* **2009**, *82*, 793−805. (h) Iwamoto, T.; Kobayashi, M.; Uchiyama, K.; Sasaki, S.; Nagendran, S.; Isobe, H.; Kira, M. *J. Am. Chem. Soc.* **2009**, *131*, 3156−3157. (i) Fukazawa, A.; Li, Y. M.; Yamaguchi, S.; Tsuji, H.; Tamao, K. *J. Am. Chem. Soc.* **2007**, *129*, 14164−14165. (j) Bejan, I.; Scheschkewitz, D. *Angew. Chem., Int. Ed.* **2007**, *46*, 5783−5786.

(3) C═P, P═P, and Si═P: (a) Li, B. L.; Matsuo, T.; Fukunaga, T.; Hashizume, D.; Fueno, H.; Tanaka, K.; Tamao, K. *Organometallics* **2011**, *30*, 3453−3456. (b) Li, B. L.; Matsuo, T.; Hashizume, D.; Fueno, H.; Tanaka, K.; Tamao, K. *J. Am. Chem. Soc.* **2009**, *131*, 13222−13223. (c) Wright, V. A.; Patrick, B. O.; Schneider, C.; Gates, D. P. *J. Am. Chem. Soc.* **2006**, *128*, 8836−8844. (d) Smith, R. C.; Protasiewicz, J. D. *J. Am. Chem. Soc.* **2004**, *126*, 2268−2269. (e) Smith, R. C.; Protasiewicz, J. D. *Eur. J. Inorg. Chem.* **2004**, *2004*, 998−1006. (f) Wright, V. A.; Gates, D. P. *Angew. Chem., Int. Ed.* **2002**, *41*, 2389−2392.

(4) (a) West, R.; Fink, M. J.; Michl, J. *Science* **1981**, *214*, 1343−1344. (b) Brook, A. G.; Abdesaken, F.; Gutekunst, B.; Gutekunst, G.; Kallury, R. K. *J. Chem. Soc., Chem. Commun.* **1981**, 191−192. (c) Yoshifuji, M.; Shima, I.; Inamoto, N.; Hirotsu, K.; Higuchi, T. *J. Am. Chem. Soc.* **1981**, *103*, 4587−4589.

(5) Some pertinent reviews: (a) Sasamori, T.; Tokitoh, N. *Bull. Chem. Soc. Jpn.* **2013**, *86*, 1005−1021. (b) Kira, M. *Proc. Jpn. Acad., Ser. B* **2012**, *88*, 167−191. (c) Scheschkewitz, D. *Chem. Lett.* **2011**, *40*, 2−11. (d) Power, P. P. *Nature* **2010**, *463*, 171−177. (e) Fischer, R. C.; Power, P. P. *Chem. Rev.* **2010**, *110*, 3877−3923. (f) Sekiguchi, A. *Pure Appl. Chem.* **2008**, *80*, 447−457. (g) Power, P. P. *Organometallics* **2007**, *26*, 4362−4372. (h) Kira, M.; Iwamoto, T. *Adv. Organomet. Chem.* **2006**, *54*, 73−148. (i) Power, P. P. *Chem. Commun.* **2003**, 2091−2101. (j) Power, P. P. *Chem. Rev.* **1999**, *99*, 3463−3503. (k) Driess, M.; Grützmacher, H. *Angew. Chem., Int. Ed. Engl.* **1996**, *35*, 828−856. (l) Tsumuraya, T.; Batcheller, S. A.; Masamune, S. *Angew. Chem., Int. Ed. Engl.* **1991**, *30*, 902−930.

(6) (a) Trinquier, G.; Malrieu, J. P. *J. Am. Chem. Soc.* **1987**, *109*, 5303−5315. (b) Carter, E. A.; Goddard, W. A. *J. Phys. Chem.* **1986**, *90*, 998−1001.

(7) Kira, M. *Organometallics* **2011**, *30*, 4459−4465.

(8) Matsuo, T.; Suzuki, K.; Fukawa, T.; Li, B. L.; Ito, M.; Shoji, Y.; Otani, T.; Li, L. C.; Kobayashi, M.; Hachiya, M.; Tahara, Y.; Hashizume, D.; Fukunaga, T.; Fukazawa, A.; Li, Y. M.; Tsuji, H.; Tamao, K. *Bull. Chem. Soc. Jpn.* **2011**, *84*, 1178−1191.

(9) Auer, D.; Strohmann, C.; Arbuznikov, A. V.; Kaupp, M. *Organometallics* **2003**, *22*, 2442−2449.

DOI: 10.1021/jacs.5b10113
J. Am. Chem. Soc. 2015, 137, 15026−15035

(10) (a) Meier, H.; Stalmach, U.; Kolshorn, H. *Acta Polym.* **1997**, *48*, 379−384. (b) Zhu, X. Z.; Tsuji, H.; Navarrete, J. T. L.; Casado, J.; Nakamura, E. *J. Am. Chem. Soc.* **2012**, *134*, 19254−19259.
(11) Lakowicz, J. R. *Principles of Fluorescence Spectroscopy*; 3rd ed.; Springer: New York, 2006.
(12) Turro, N. J. *Modern Molecular Photochemistry*; University Science Books: Sausalito, CA, 1991.
(13) Meier, H. *Angew. Chem., Int. Ed.* **2005**, *44*, 2482−2506.
(14) Shepherd, B. D.; West, R. *Chem. Lett.* **1988**, 183−186.
(15) Kira, M.; Ishima, T.; Iwamoto, T.; Ichinohe, M. *J. Am. Chem. Soc.* **2001**, *123*, 1676−1682.
(16) Frisch, M. J.; Trucks, G. W.; Schlegel, H. B.; Scuseria, G. E.; Robb, M. A.; Cheeseman, J. R.; Scalmani, G.; Barone, V.; Mennucci, B.; Petersson, G. A.; Nakatsuji, H.; Caricato, M.; Li, X.; Hratchian, H. P.; Izmaylov, A. F.; Bloino, J.; Zheng, G.; Sonnenberg, J. L.; Hada, M.; Ehara, M.; Toyota, K.; Fukuda, R.; Hasegawa, J.; Ishida, M.; Nakajima, T.; Honda, Y.; Kitao, O.; Nakai, H.; Vreven, T.; Montgomery, J. A., Jr.; Peralta, J. E.; Ogliaro, F.; Bearpark, M.; Heyd, J. J.; Brothers, E.; Kudin, K. N.; Staroverov, V. N.; Kobayashi, R.; Normand, J.; Raghavachari, K.; Rendell, A.; Burant, J. C.; Iyengar, S. S.; Tomasi, J.; Cossi, M.; Rega, N.; Millam, N. J.; Klene, M.; Knox, J. E.; Cross, J. B.; Bakken, V.; Adamo, C.; Jaramillo, J.; Gomperts, R.; Stratmann, R. E.; Yazyev, O.; Austin, A. J.; Cammi, R.; Pomelli, C.; Ochterski, J. W.; Martin, R. L.; Morokuma, K.; Zakrzewski, V. G.; Voth, G. A.; Salvador, P.; Dannenberg, J. J.; Dapprich, S.; Daniels, A. D.; Farkas, Ö.; Foresman, J. B.; Ortiz, J. V.; Cioslowski, J.; Fox, D. J. *Gaussian 09*, Revision B.01; Gaussian, Inc.: Wallingford CT, 2010.
(17) Sizova, O. V.; Skripnikov, L. V.; Sokolov, A. Y. *J. Mol. Struct.: THEOCHEM* **2008**, *870*, 1−9.
(18) Reed, A. E.; Curtiss, L. A.; Weinhold, F. *Chem. Rev.* **1988**, *88*, 899−926.

DOI: 10.1021/jacs.5b10113
J. Am. Chem. Soc. 2015, 137, 15026−15035